Available online at www.sciencedirect.com
ScienceDirect
Catalysis Today 130 (2008) 327–336
CATALYSIS TODAY
www.elsevier.com/locate/cattod

CoMo/MgO–Al_2O_3 supported catalysts: An alternative approach to prepare HDS catalysts

F. Trejo, Mohan S. Rana *, J. Ancheyta

Instituto Mexicano del Petróleo, Eje Central Lázaro Cárdenas 152, Mexico D.F. 07730, Mexico

Available online 3 December 2007

Abstract

Three different supports were prepared with distinct magnesia–alumina ratio $x = MgO/(MgO + Al_2O_3) = 0.01$, 0.1 and 0.5. Synthesized supports were impregnated with Co and Mo salts by the incipient wetness method along with 1,2-cyclohexanediamine-*N*,*N*,*N*′,*N*′-tetraacetic acid (CyDTA) as chelating agent. Catalysts were characterized by BET surface area, Raman spectroscopy, SEM-EDX and HRTEM (STEM) spectroscopy techniques. The catalysts were evaluated for the thiophene hydrodesulfurization reaction and its activity results are discussed in terms of using chelating agent during the preparation of catalyst. A comparison of the activity between uncalcined and calcined catalysts was made and a higher activity was obtained with calcined MgO–Al_2O_3 supported catalysts. Two different MgO containing calcined catalysts were tested at micro-plant with industrial feedstocks of heavy Maya crude oil. The effect of support composition was observed for hydrodesulfurization (HDS), hydrodemetallization (HDM), hydrodeasphaltenization (HDAs) and hydrodenitrogenation (HDN) reactions, which were reported at temperature of 380 °C, pressure of 7 MPa and space-velocity of 1.0 h^{-1} during 204 h of time-on-stream (TOS).

Keywords: Chelating agent; Al_2O_3–MgO supported catalysts; Maya crude hydrotreating

1. Introduction

Environmental regulations are focusing in reducing the level of pollutants by diminishing at lower level of sulfur, nitrogen and metals (particularly Ni and V) contents in commercial fuels. For this reason, refiners need to decrease the concentration of contaminants such as sulfur in petroleum fractions particularly gasoline and middle distillates. Hydrodesulfurization is an important hydrotreating process (HDT) by which this target can be reached by modifying the support properties of the catalysts or by increasing the severity of the reaction. Among them, the modification of the support particularly mixed oxides and catalyst properties is more suitable and less expensive [1,2]. The use of mixed oxides is not new, which assessed the catalytic functionalities of sulfided CoMo catalysts, and their dependence on the nature of the support and incorporation of additives. Common supports for hydrodesulfurization of petroleum are alumina-based [3]. The incorporation of MgO, SiO_2, TiO_2 and ZrO_2 with Al_2O_3 modifies the nature of active phase interactions on the support surface [4]. Therefore, these oxides play a structural promoting role to the support contribution and its interaction towards the active metal [5].

Particularly MgO–Al_2O_3, recently [6–10] showed that the support basicity might be favorable increasing the interaction between support and acidic molybdenum species (MoO_3). Therefore, the use of MgO–Al_2O_3 as a basic support can present a wide range of textural properties making it useful as a support for HDT catalysts. Apart from the support composition, remarkable improvements in HDS activity of CoMo and NiMo catalysts can be achieved by the addition of chelating agent during the preparation of catalysts [11–18]. These complexing agents have been found to be very effective in the formation of highly active CoMoS sites with extremely high selectivity by suppressing Mo-support interactions. According to Cattaneo et al. [13] the role of the chelating ligand is believed to change the sulfiding mechanism of Ni by complexing with Ni, which subsequently leads to a higher dispersion of the promoter on the edges of the MoS_2 slabs. The chelating ability of the described ligands is closely related to the pH of the impregnation solution. The metal ion/chelate ratio in the complex depends on the overall metal ion/chelate ratio in solution, the presence of other ligands or metal ions and the pH. It is seen that sulfidation of the

* Corresponding author. Tel.: +52 55 9175 8418; fax: +52 55 9175 8429.
E-mail address: msingh@imp.mx (M.S. Rana).

0920-5861/$ – see front matter © 2007 Elsevier B.V. All rights reserved.
doi:10.1016/j.cattod.2007.10.105

molybdenum precursor takes place at temperatures between 75 and 175 °C. In the dried catalyst prepared with nitriloacetic acid (NTA) the cobalt precursor started to sulfide at temperatures exceeding 125 °C, which was completed only at a temperature of about 225 °C [19]. van Veen et al. [20,21] reported that catalyst preparation with a chelated cobalt–NTA complex yielded catalysts containing exclusively the catalytically active CoMoS phase, whereas catalyst preparation without NTA were less active. This effect is not only restricted to NTA but also a wide range of chelating agents was able to improve the formation of the highly active phase [11]. The role of different chelating agents is discussed in several papers. Chelating agents such as CyDTA, EDTA, TTHA, NTA, DTPA and citric acid, among other are used [22–33].

The aim of this work is to illustrate the different supports that were prepared by varying the magnesia–alumina content and thereafter impregnated with Co and Mo salts adding the complexing agent. The influence that CyDTA possesses as chelating agent in synthesizing CoMo/MgO–Al_2O_3 supported catalysts was studied for hydrotreating of thiophene model molecule as well as heavy crude oil. The calcined catalysts resulted more active than uncalcined catalysts. Catalysts were evaluated in the thiophene HDS as preliminary screening after that the better catalyst were evaluated at micro-plant scale with Maya crude.

2. Experimental

2.1. Supports and catalysts preparation

A set of three MgO–Al_2O_3 supports was synthesized by homogeneous precipitation using aqueous solution of aluminum nitrate, magnesium nitrate and precipitating agent 10% NH_4OH solution and controlling the pH at 9.2. After that, the solution was filtered and the precipitated was dried at room temperature. Finally, the calcination of supports was done at 550 °C during 4 h. MgO–Al_2O_3 material was denoted as Mg–Al. The Mg–Al-0.01, Mg–Al-0.1, Mg–Al-0.5 supports corresponded to 1 wt.%, 10 wt.% and 50 wt.% MgO, respectively. Supports were impregnated by incipient wetness impregnation with a constant molar ratio of [Co/(Co + Mo)] = 0.4. MgO–Al_2O_3 supported Mo was obtained by adding a solution of ammonium heptamolybdate.

The MgO–Al_2O_3 supported CoMo–CyDTA catalysts were prepared by the incipient wetness impregnation of solutions containing the Co, Mo and CyDTA salts using appropriate amount of $Co(NO_3)_2{\cdot}6H_2O$, ammonium heptmolybdate and 1,2-cyclohexanediamine-*N*,*N*,*N*′,*N*′-tetraacetic acid, respectively. In all preparations, a molar ratio of CyDTA/Co = 1.2 was used and a pH of 9.5 was maintained during the incorporation of CyDTA, because chelating agent forms a stable complex with Co at pH > 8.5 [34]. After impregnation, the catalysts were dried at room temperature overnight and then at 120 °C for 12–15 h. Calcination of the catalysts was achieved at 450 °C during 4 h with a heating rate of 1 °C/min. Catalysts were denominated as CoMo/Mg–Al-0.01, CoMo/Mg–Al-0.1, CoMo/Mg–Al-0.5.

2.2. Catalysts characterization

Fresh and spent catalysts were characterized by BET specific surface area, pore volume and average pore diameter. The samples were out-gassed for 3 h at 300 °C prior to the adsorption. Tests were carried out in a Quantachrome Nova 4000 equipment using nitrogen gas for measurements at −196 °C. The composition of catalysts was studied by means of elemental analysis with the SEM-FIB analytical instrument xT Nova NanoLab 200 (FEI Schottky FEG, 30-1 keV) combined with a dual high resolution focused ion beam (Ga^+ FIB) using a detector type SUTW Sapphire with LEAP+ crystals for the best light element performance of the Si(Li) detector. The sample was deposited on a carbon holder and evacuated at high vacuum (10^{-10} mbar). The analysis was carried out across the radial line of the extrudate and five points were chosen, i.e. external, semi-external, center and vice-versa. The Raman spectra were performed on T64000 spectrometer (Jobin Yvon Horiba). This instrument is combined with a microscope (Olympus, BX41), with an argon ion laser operating at 514.5 nm at a power level of 5 mW. The spectrometer is equipped with a CCD camera detector.

The mapping of the elements was carried out for the support (Mg and Al) and spent catalyst (Co, Mo, Ni, V and S) by scanning transmission electron microscopy (STEM). TEM observations of spent catalyst were analyzed using a JEOL JEM 2200FS transmission electron microscope, with a 200 kV electron beam with an energy dispersion analyzer (EDS). The microscope is equipped with a field emission gun (FEG). Samples were milled in an agate mortar and ultra sonically suspended in *n*-heptane. A drop of the supernatant liquid was taken and placed on a 3 mm diameter lacey copper grid coated with a sputtered carbon polymer. STEM images were recorded using an annular dark-field detector, giving a signal that is sensitive to the atomic number in the support (Al*k* and Mg*k*) or spent catalysts (Ni*k* and V*k*). Five different zones were estimated for STEM of elemental mapping analysis. For TEM, at least 12 representative micrographs were taken for each catalyst in high-resolution mode. While an average length (L_{av}) and number of the stacks (N_{av}) of MoS_2 more than 200 crystallites were measured on different images.

2.3. Catalysts evaluation

Preliminary screenings of catalysts were carried out by evaluating them for thiophene HDS in a glass reactor using a weight of catalyst of 200 mg. The catalysts were presulfided using a mixture of CS_2/H_2 with a 10% CS_2 and 90% H_2 ratio. After sulfidation, thiophene HDS experiments were conducted at 400 °C with a flow of thiophene + H_2 of 100 mL/min keeping constant thiophene saturator temperature at 5 °C in order to achieve 4.7 mol % of thiophene. The products were analyzed online using a FID gas chromatograph. The conversions were kept low to operate in differential regime. A first-order reaction rate was considered for thiophene conversion.

CoMo/Mg–Al-0.01 and CoMo/Mg–Al-0.1 calcined catalysts were thereafter evaluated at micro-plant scale using a fixed

Table 1
Properties of the Maya crude

Properties of Maya crude	
Composition	
C (wt.%)	86.9
H (wt.%)	5.3
N (wt.%)	0.3
S (wt.%)	3.52
Ni (ppm)	49.5
V (ppm)	273.0
n-C_7 insolubles (wt.%)	12.7
Density, 20/4 °C	0.9251
Ramsbottom carbon (wt.%)	10.87
API gravity	21.31

bed reactor operating at up-flow mode with Maya crude as feedstock. Properties of the feedstock are shown in Table 1. 10 mL of oxide catalyst (cylindrical extrudates) was loaded with inert material (SiC). Catalysts were previously dried at 120 °C for 2 h and then wetted with straight-run gas oil (SRGO) at 150 °C during 2 h. Finally, catalysts were sulfided in situ with a sulfiding feed containing ~2.0 wt.% sulfur (1 wt.% DMDS + SRGO) at 2.7 MPa and 260 °C for 3 h. Temperature was rose up to 320 °C and kept constant during 5 h at the same pressure. Once catalyst was sulfided, the Maya crude was fed to the reactor at 7 MPa and 380 °C. LHSV was adjusted at 1.0 h^{-1} with 9.6 L/h of H_2 to keep the H_2/HC ratio at 890 m^3/m^3 and periodic sampling was carried out every 12 h during 204 h.

Metals (Ni, V) in hydrotreated products and metals deposition on spent catalysts were measured by atomic absorption by using the ASTM-D-5863. Sulfur analysis in liquid products was carried out in a Horiba SLFA-2100 analyzer by fluorescent energy dispersive X-ray fluorescence. Asphaltenes were measured by using the ASTM-D-3279 method as n-heptane insolubles. Total nitrogen content was analyzed with the ASTM-D-4629 method by oxidative combustion and chemiluminescence.

3. Results and discussion

3.1. Preparation of supports

The homogeneous precipitation method was used for support preparation and the distribution of MgO in alumina was determined by a STEM mapping of different elements as shown in Figs. 1 and 2. The qualitative microanalysis of samples indicated that the distribution of Mg in alumina matrix is evenly dispersed at nano-scales. These results indicated that

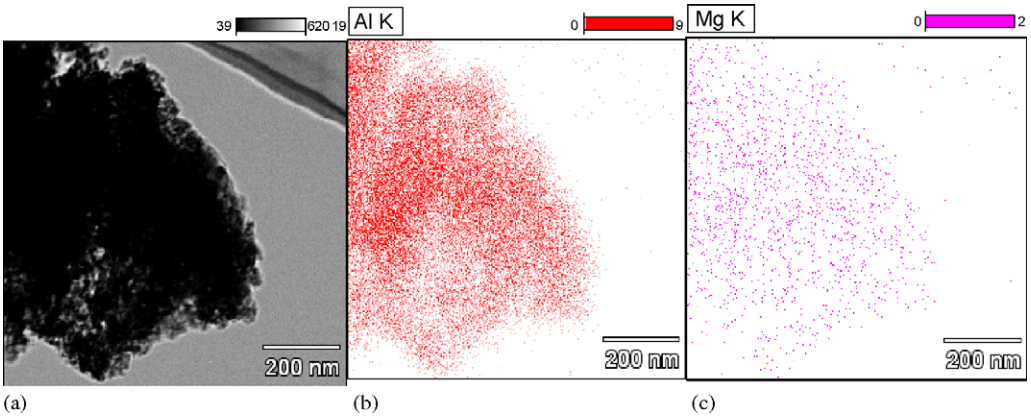

Fig. 1. Scanning transmission electron micrographs (STEM) and qualitative nano-microanalysis of mixed oxide support (1.5 wt.% MgO): (a) sample image, (b) Al distribution and (c) Mg distribution.

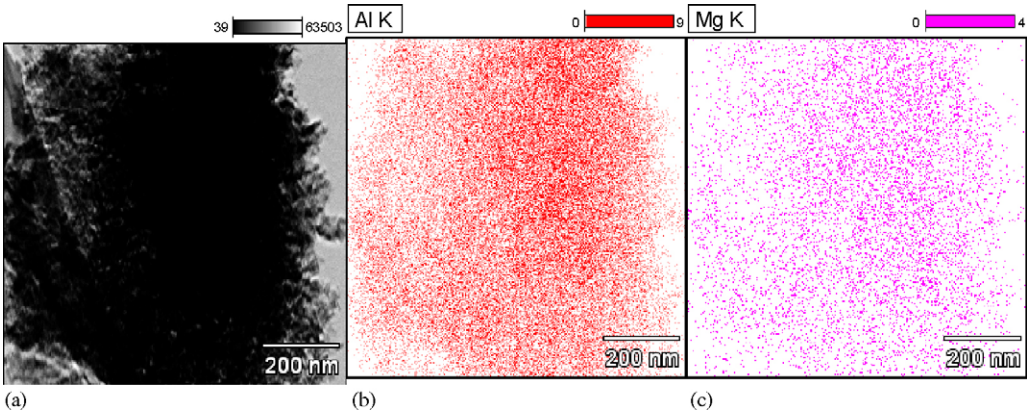

Fig. 2. Scanning transmission electron micrographs (STEM) and qualitative nano-microanalysis of mixed oxide support (9.4 wt.% MgO): (a) sample image, (b) Al distribution and (c) Mg distribution.

the bulk precipitation could be avoided by using NH_4OH precipitation, and at our support preparation conditions. The structural morphology of mixed oxides by using electron mapping is to confirm an exact nature of mixed oxide components in solid state. STEM is one of the techniques to isolate electrons, which gives useful structural information at nano-scale. However, to confirm the qualitative analysis scanning electron microscope of the energy dispersive X-ray was performed. SEM-EDX results are given in Table 2 from which it is seen that real composition is very similar to the theoretical values. The preparation of MgO oxide is sensitive to the precipitation conditions, for instance at lower pH or even very high pH the magnesium will remain un-precipitated in the solution. The ample precipitations of two components Mg–Al at our preparation conditions were obtained at pH 9.2.

3.2. Catalyst characterization

Fresh catalysts were characterized by BET method for textural properties, which are shown in Table 2. Fig. 3 presents the pore size distribution of the catalysts. This figure indicates that optimum MgO content to generate large pore diameter is 10 wt.% MgO, since CoMo/Mg–Al-0.1 supported catalyst demonstrated macropores while the others are mesoporous in nature. Usually, the generation of textural properties is the innate property of the support, which is a result of number of hydroxyl groups and interaction between the two components of mixed oxide in aqueous medium. The impregnation of active metals (Co and Mo) may also influence (decrease) particularly the textural property but its effect is very low particularly at low loading of metal.

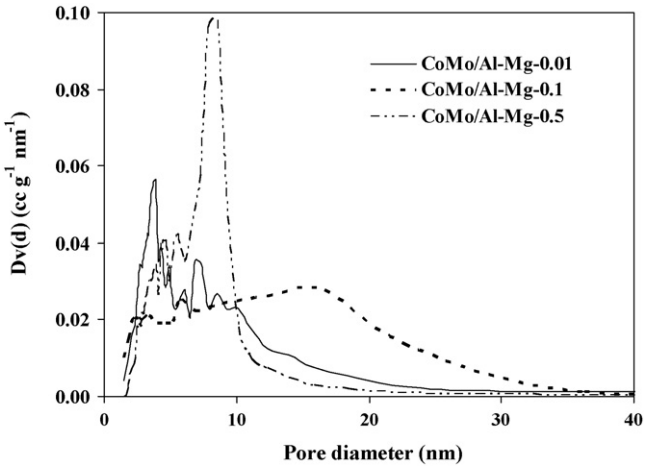

Fig. 3. Effect of support composition on the textural properties of CoMo supported catalysts.

The fresh catalyst composition was determined by using SEM-EDX and atomic absorption analyses. Both values are very close and the results are shown in Table 2. Similarly the oxide catalyst composition is shown in Fig. 4. EDX microanalysis of the catalyst at different points of the catalyst particles revealed a homogeneous distribution of elements, which is probably due to the low loading and the preparation method adopted. The presence of Co, Al, Mg and O has been identified with their main Kα EDX emission. The emission peak at 2.3 keV (MoL) against the peak 17.5 keV (Mo Kα) is relatively wider suggesting that the Mo may exist in two different electronic environments over the support surface,

Table 2
Properties of fresh and spent catalysts

Properties	CoMo/Mg–Al-0.01		CoMo/Mg–Al-0.1		CoMo/Mg–Al-0.5
	Fresh	Spent	Fresh	Spent	Fresh
Textural properties					
SSA (m^2/g)	219	78	234	124	186
PV (cm^3/g)	0.41	0.18	0.56	0.27	0.51
APD (nm)	7.4	6.3	9.5	8.6	10.9
Pore availability (%)					
Micropores	5.2	1.1	6.0	0.8	0.6
Mesopores	86.2	87.6	93.4	98.2	98.8
Macropores	8.6	11.3	0.6	1.0	0.6
Pore size distribution (vol.%)					
<2 nm	5.2	1.1	6.0	0.8	0.6
2–5 nm	15.6	17.8	7.3	13.5	5.6
5–10 nm	34.1	32.2	27.4	40.8	25.7
10–25 nm	29.6	26.1	55.0	42.0	64.6
25–50 nm	6.9	11.5	3.7	1.8	3.0
50–100 nm	5.8	6.8	0.4	0.6	0.3
>100 nm	2.8	4.5	0.2	0.4	0.3
Catalyst composition (wt.%)					
CoO (Co)	4 (3.1)	–	4.1 (3.2)	–	3.9 (3.9)
MoO_3 (Mo)	9.4 (6.3)	–	10 (6.7)	–	9.8 (6.5)
Support composition (SEM-EDX) (wt.%)					
MgO	1.5	–	9.4	–	43.9
Al_2O_3	98.5	–	91.6	–	56.1

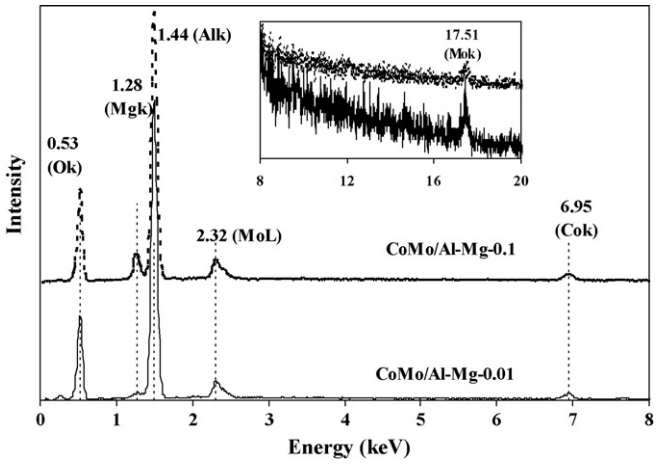

Fig. 4. EDX spectra of the CoMo catalysts supported on $MgO–Al_2O_3$.

which is particularly possible in the case of mixed oxide supports.

To identify the surface species interaction with the support, Raman spectroscopy of the oxide catalysts characteristic peaks intensities are shown in Fig. 5. The intensity of two different catalysts does not match with each other that might be due to the support composition and the interaction of the Mo species in different electronic environment. Similar results were reported for changes in support such as MgO and alumina [10,35], in which a displacement of the signal up to 924 cm^{-1} on pure magnesia supported catalysts has been found. In our case, the support has 10 wt.% of MgO which could influence the apparition of the signal at this value because of higher MgO in the support. The bands at around 945 and 919 cm^{-1} may correspond to magnesium molybdate formation. The surface molybdenum species supported on magnesia have been reported at 855, 907, 915, 967 and 1094 cm^{-1} [35–37]. Both catalysts show similar Raman patterns, however, lower intensity of signals is present in higher magnesium containing catalyst (Fig. 5). The catalysts also showed one peak at around 221 cm^{-1} that corresponds to Mo–O symmetric stretch and appears due to the Mo–O–Mo deformation and is symptomatic of polymolybdate species as reported by Griffith [38]. Moreover, a small shoulder at 981 cm^{-1} appears when a peak at 221 cm^{-1} is present that could be also assigned to the symmetric Mo–O stretch as stated by Chang et al. [39]. These results confirmed that Mo species observed by Raman IR spectroscopy was $MgMoO_4$ and that indicates that Mo ions react easily with subsurface layers of MgO, which further exclude the possibility to bulk MoO_3 and its interaction with Co in the form of $CoMoO_4$.

4. Catalytic activities

4.1. Thiophene activity

Results of the catalysts activity were compared with an alumina-supported CoMo catalyst prepared with complexing agent. Two states of the catalyst were evaluated: uncalcined and calcined. In the case of uncalcined sample, the weight is taken as calcined catalyst thus, after sulfidation the weight of catalysts remains the same as in the case of calcined catalyst. The MgO containing catalyst showed higher activity than alumina as shown in Fig. 6. This higher activity is due to the support effect which is well reported in the literatures [1,2,7,9,10]. The promotion for uncalcined catalyst is not comparable to the other studies reported in the literature but for calcined catalysts the activity is decreasing for alumina while for $MgO–Al_2O_3$ supported catalyst showed significant increase in HDS activity. On the other hand, the $MgO–Al_2O_3$ supported calcined catalyst exhibited higher HDS activity than uncalcined, which is rather strange because the chelating agent catalysts have been reported to be lower active in calcined state [40,41]. With respect to catalytic activities the optimum magnesia content in the support was found to be 10 wt.%, most likely due to the better dispersion and morphology of the active components at this Mg content. The higher activity during the thiophene HDS of the catalysts prepared with chelating agents could be attributed to the formation of polymolybdates which can be

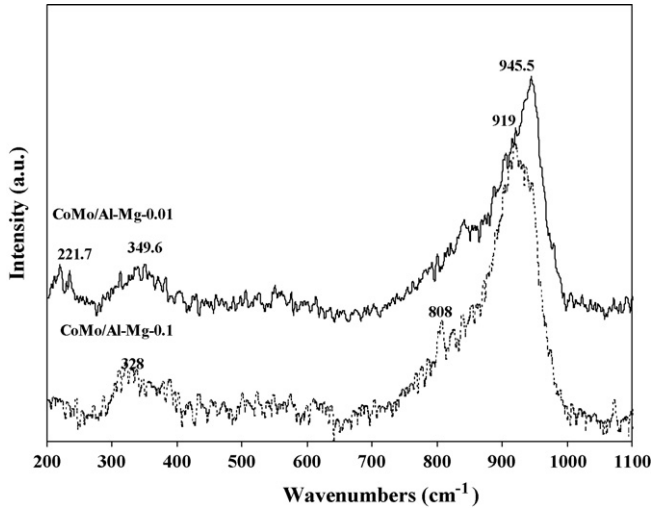

Fig. 5. Raman spectra of CoMo catalysts supported on $MgO–Al_2O_3$.

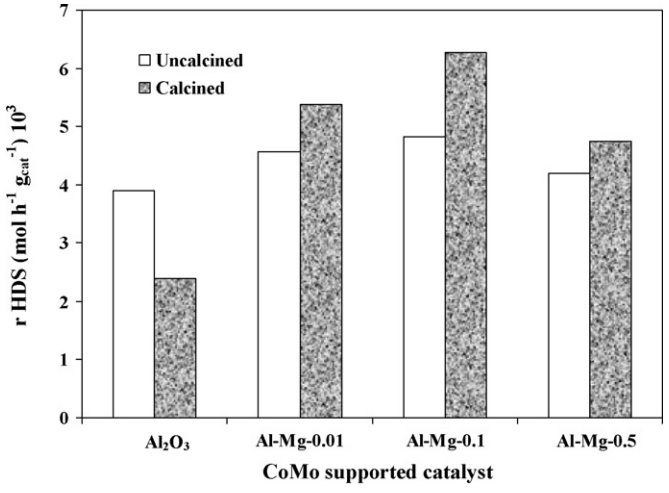

Fig. 6. Effect of support and catalysts calcination on the thiophene HDS using chelating agent during the preparation ($CoMo/MgO–Al_2O_3$).

easily sulfided to create MoS_2 crystallites. The sulfidation of the Co after Mo leads to higher coverage on the edges over molybdenum nano-crystallites creating the highly active CoMoS phases. Recently, Rana et al. [40] have reported that the effectiveness of the chelating agent improves the promotion of Mo by Co. van Dillen et al. [19] have stated that catalysts are retarded to be sulfided when the deposited molybdate and cobalt ions interact strongly with the support. Usually, the chelating agent (Co-complex) is destroyed during calcination, which enhances an earlier sulfidation of the Co phase, or Co sulfides prior to the molybdenum, such catalyst results in inferior promotion of MoS_2 by Co and lower HDS activity. However, this effect was studied either for alumina supported catalyst or for SiO_2, those supports have relatively lower isoelectric point (IEP) while $MgO–Al_2O_3$ support has higher IEP, which might play a fundamental role in the anchoring of the metal precursors on the support surface. When using MgO in support it is also possible that the chelating agents have a little role to complex with surface MgO during the high impregnation pH, such complex may prevent direct interaction of Mo with the support and during calcinations Mo interacts weakly, which prevails the Co sulfidation, more CoMoS active structures are formed and consequently enhanced catalytic activities are obtained. The activity results are in agreement with Raman spectrum that the diffusion of Co in alumina support is not seen. Raman intensity has been deducted for $MoMgO_4$ at 960 cm^{-1} [39]. However, there are not straight results reported for sulfidation of $MgMoO_4$ but it appears that the surface magnesium molybdate sulfides at the usual or may be little lower temperature compared with the $CoMo/\gamma–Al_2O_3$ [40]. Thus the results indicated that chelating agent prevails the CoMoS sites rather than the interaction with the support or molybdenum. On the other hand, uncalcined catalyst may delay the sulfidation of Mo, which may either weakly sulfide the catalyst or decrease the promotional effect.

Apart from the enhanced thiophene HDS activity, the calcined catalyst can be effectively used for heavy oil hydroprocessing because uncalcined chelating agent catalysts have adverse effect on reactor operation due to the decomposition of chelating agent, which produces highly viscous substances.

4.2. Maya crude hydrotreating

The screening of the catalysts for the thiophene HDS allowed us to select the better catalyst, which presented higher activity. However, the behavior of these catalysts may not be the same as for thiophene because the heavy oil catalyst is more affected by the pore diameter rather than metal dispersion [42]. Nevertheless, CoMo/Mg–Al-0.01 and CoMo/Mg–Al-0.1 catalysts were chosen to be evaluated at micro-plant scale with Maya crude as feedstock at conditions similar to industrial ones. According to the textural properties, the CoMo/Mg–Al-0.1 catalyst possesses large diameter of pores (Fig. 3), they are distributed in the mesoregion and that may prevail heavy crude oil activity more effectively. CoMo/Mg–Al-0.01 has relatively lower pores which are responsible of the lower activity

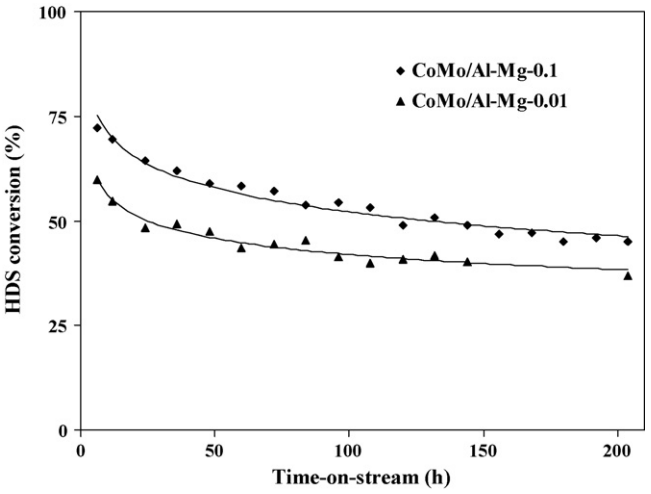

Fig. 7. HDS of Maya crude with CoMo/Mg–Al-0.01 and CoMo/Mg–Al-0.1 calcined catalysts.

compared with CoMo/Mg–Al-0.1. The later catalyst possesses about 50% of its pores in the range of 10–25 nm. Its specific surface area is lower compared with CoMo/Mg–Al-0.01, which is in agreement with the pore size.

The heavy oil hydrodesulphurization activity for the two catalysts with time-on-stream is shown in Fig. 7. The CoMo/Mg–Al-0.01 catalysts showed lower activity than that of CoMo/Mg–Al-0.1. The activity difference between the two catalysts could be either due to the MgO content in support or due to the larger pore of the catalyst. However, the activity decrease with time remains the same for both catalysts, which indicated that the MgO may have effect on hydrodrogenolysis of C–S bond. Similar tendency for HDN activity is observed as shown in Fig. 8. In the crude oil most of the nitrogen is present in the form of porphyrinic structures so that larger pores are necessary to process such kind of complex molecules. Thus, if we calculate the two catalysts activity ratio (CoMo/Mg–Al-0.1/CoMo/Mg–Al-0.01), for HDS (i.e. 1.2) and HDN (i.e. 2.1), the

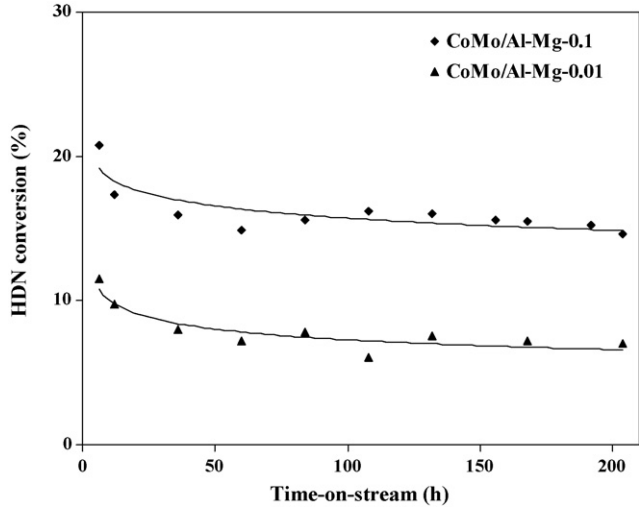

Fig. 8. HDN of Maya crude with CoMo/Mg–Al-0.01 and CoMo/Mg–Al-0.1 calcined catalysts.

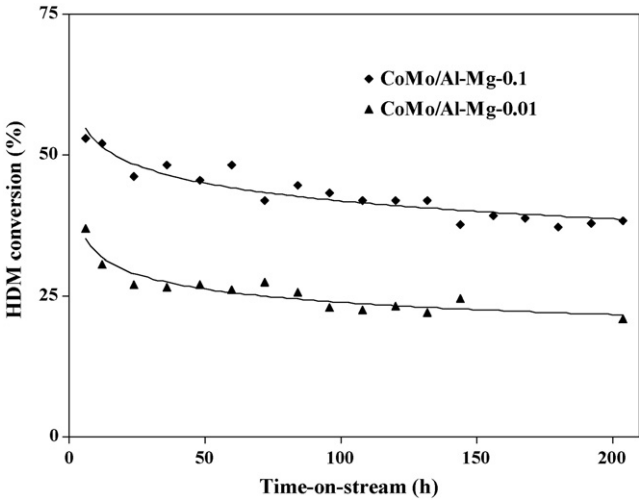

Fig. 9. HDM of Maya crude with CoMo/Mg–Al-0.01 and CoMo/Mg–Al-0.1 calcined catalysts.

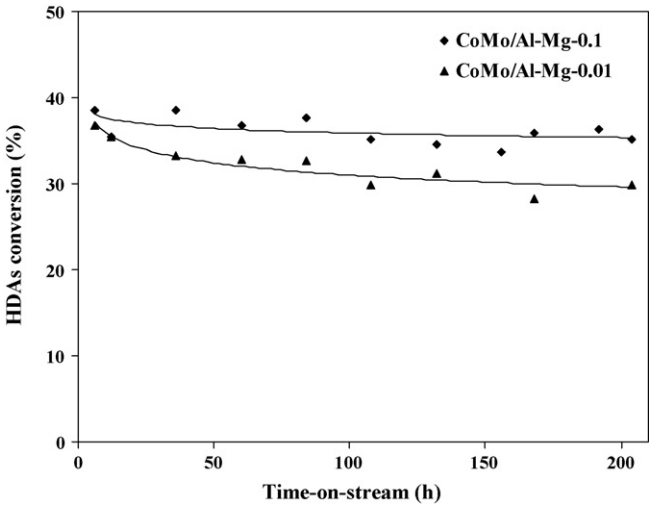

Fig. 10. HDAs of Maya crude with CoMo/Mg–Al-0.01 and CoMo/Mg–Al-0.1 calcined catalysts.

ratios indicated that the difference between the two catalyst is due to the pore diameter and plays an important role to control the catalytic activity. Due to the higher ratio of HDN that corresponds to the large pores, it can be stated that the reaction takes place within the interval of meso and macrorange of pores.

Metals removal as function of the time-on-stream is observed in Fig. 9. Results obtained from HDM evidences that a good stability of the catalyst is obtained even after 200 h of time-on-stream reaching almost a constant HDM conversion. The Ni and V metals are considered for HDM, which are commonly complexes with porphyrinic structures. The complexed metals molecules are either in free state in crude oil or sandwiched between the asphaltene structures, in both cases these molecules are huge in nature [42]. Hence, wide pore catalysts are recommended when processing this kind of molecules at the expense of reducing the specific surface area and in consequence lowering the HDS activity. For this reason, bimodal catalysts would be preferred because HDS occurs effectively in smaller pores whereas HDM takes place in larger pores as reported previously by Rana et al. [43] during the hydroprocessing of heavy crude. Increasing the pore size improves the diffusion but surface area decreases by which a compromise between surface area and pore diameter is essential in selecting catalysts for heavy crude oil and residue hydroprocessing [44].

The hydrodeasphaltenization results in Fig. 10 indicate that the asphaltenes are intimately related to complex metals. The reduction with time-on-stream for HDAs activity is relative less affected compared with those observed for HDS, HDM and HDN reactions. The less deactivation could be due to the MgO in the catalyst, which is owed to the basic nature of catalyst. The difference in the behavior of the two catalysts is most likely due to the relatively high MgO content in the catalyst and larger pore diameter that promotes large asphaltene molecules diffusion and at the same time has lower hydrocracking and hydrogenation functions [5]. The stability of CoMo/Mg–Al-0.1 catalyst with time-on-stream confirms the role of MgO along with large pore diameter. It seems that large pores are worthless for HDM and HDAs, that is pores in the range of 10–25 nm are more useful and accessible to large molecules such as metal complexes and asphaltenes. Fig. 11 shows a comparison between the two catalyst selectivities of different reactions. It is observed that CoMo/Mg–Al-0.1 (higher MgO content) is more selective to hydrogenolysis (HDM, HDS) with respect to HDAs, which confirms that the hydrogenolysis function is more likely on the basic nature of catalyst because the HDAs reaction is also dominated by pore diameter, which is not the case of the present study.

5. Characterization of spent catalysts

Catalysts that were evaluated at micro-plant scale with Maya crude were characterized by nitrogen adsorption–desorption, atomic adsorption and HRTEM. The textural properties of spent catalysts are given in Table 2, while the quantitative

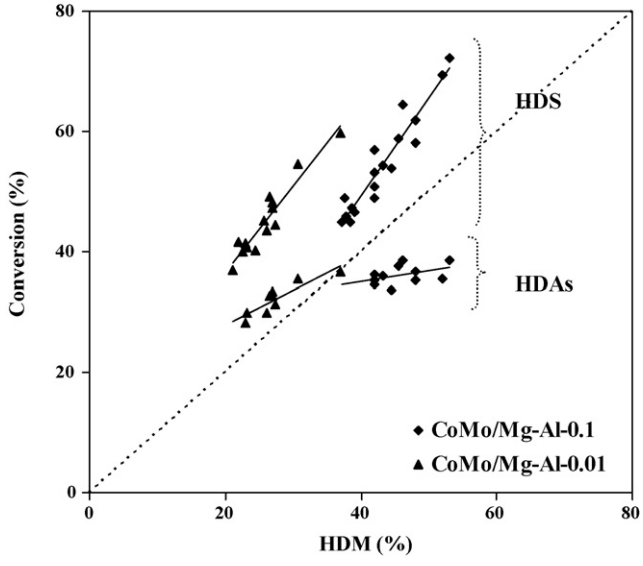

Fig. 11. Comparison between activities in different reactions.

analyses of the deposited species determined by atomic absorption are presented in Table 3. In spent catalysts the deposited species reduces the SSA (50–60%) and total pore volume (50–55%). The reduction was higher in the case of CoMo/Mg–Al-0.01 catalyst than in CoMo/Mg–Al-0.1 as a consequence mainly of the deposition of carbon in the pores and also due to the blockage of macropores, which are relatively more abundant in the CoMo/Mg–Al-0.01 catalyst. The qualitative analysis of Ni and V on spent catalysts is estimated using scanning transmission electron microscope

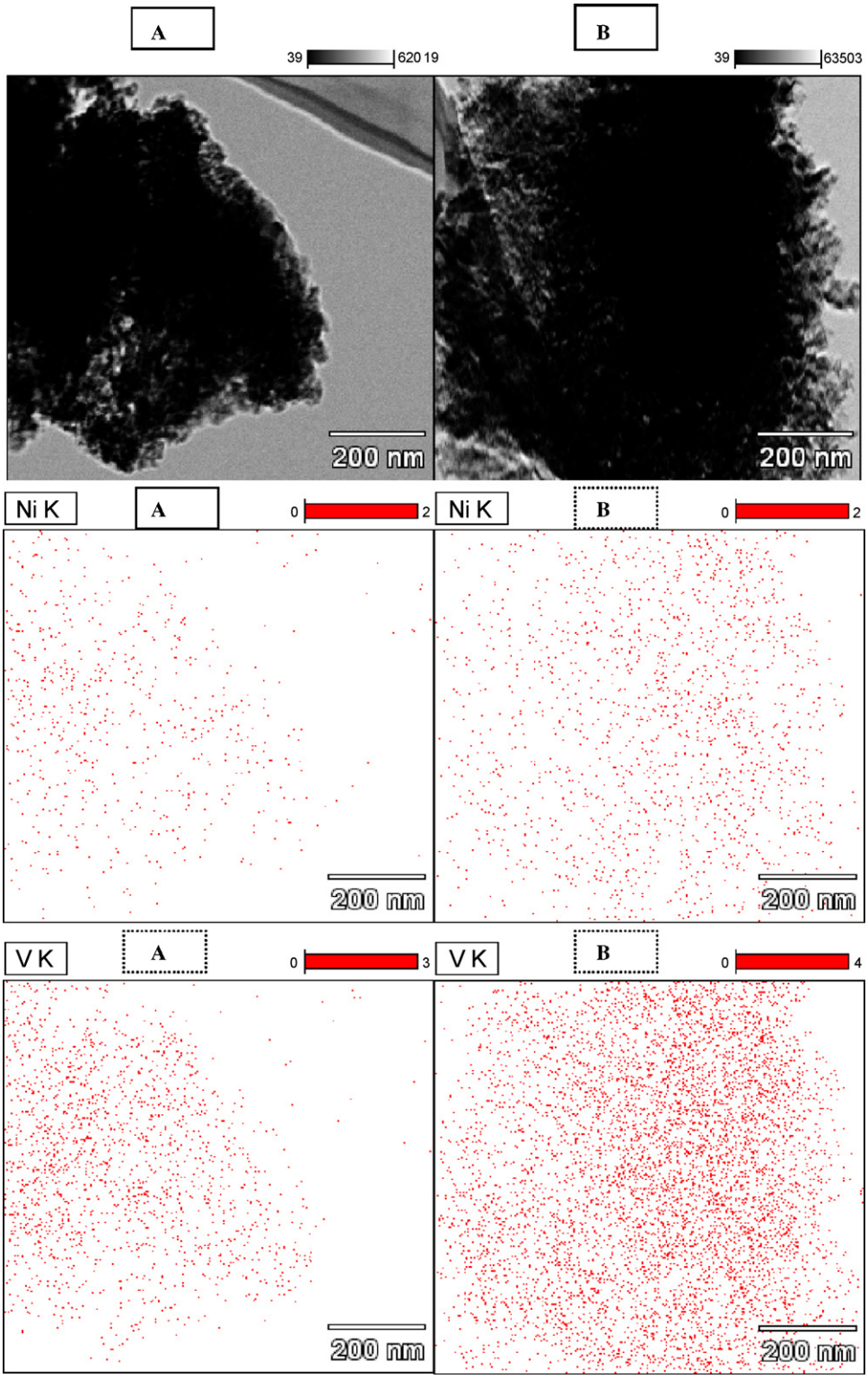

Fig. 12. Scanning transmission electron micrographs (STEM) and qualitative nano-microanalysis of Ni and V distribution: (A) 1.5 wt.% MgO (7.4 nm, APD) and (B) 9.4 wt.% MgO (9.5 nm, APD) in support.

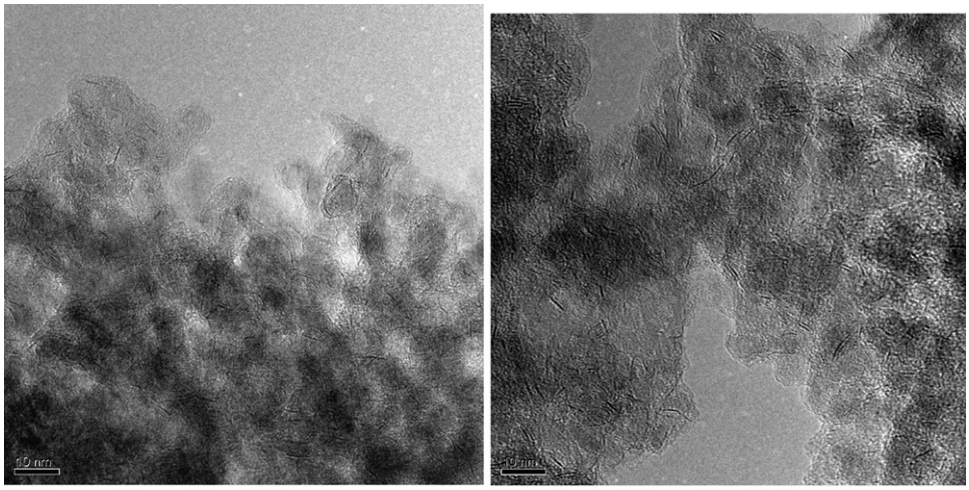

Fig. 13. TEM analysis of spent catalysts: (A) 1.5 wt.% MgO and (B) 9.4 wt.% MgO in support.

(STEM) images and element mappings are shown in Fig. 12. The element image of Ni and V atom distribution is indicating that all of the Ni and V were consistently deposited. However, the large pore diameter catalyst (CoMo/Mg–Al-0.1) has more Ni and V, which is in agreement to the quantitative results obtained by atomic absorption (Table 3). Additionally, it appears the crystal size of VxSy is preferentially associated with the Ni or even Co and Mo sulfided and unsulfided system [45]. The spent catalysts TEM is shown in Fig. 13. The MoS_2 stacking layers partially remain evident after 204 h of time-on-stream, which indicated that the catalyst could be further used effectively. However, higher MgO containing catalyst (CoMo/Mg–Al-0.1) has relatively higher MoS_2 average stacking ($N_{av} = 1.5$) and average slab length ($L_{av} = 3.5$) while CoMo/Mg–Al-0.01 catalyst has $N_{av} = 1.1$ and $L_{av} = 3.3$ nm. The absence of multilayer MoS_2 slabs on spent catalysts is distracted under the reaction conditions by mechanical stress or chemical interactions such as Ni and V sulfide. The MoS_2 slabs are isolated and parts of these are in accordance with values derived from STEM results (Fig. 12), in which the MoS_2 particle size increased [46]. However, the particle size and larger particles will depend on the catalyst pore diameter and that indeed induces deactivation, as demonstrated in Figs. 9–11. The CoMo/Mg–Al-0.1 catalyst possesses a higher capacity of metals retention which in the case of vanadium is twice higher than CoMo/Mg–Al-0.01 (Table 3). Nickel was also deposited in slightly higher amount in CoMo/Mg–Al-0.1 than CoMo/Mg–Al-0.01, while carbon deposition was higher in CoMo/Mg–Al-0.01 than in CoMo/Mg–Al-0.1 catalyst. A possible explanation for this fact is that CoMo/Mg–Al-0.1 has a bigger amount of mesopores and contains higher amount of MgO, which represents basic nature of catalyst. The lower coke formation is in accordance to the better stability of catalyst particularly for HDAs (Fig. 10). It is considered that asphaltenes are coke precursors and they are polydisperse (molecules of different sizes), thus the smaller molecules can penetrate and react in small pores, however restrictions related to diffusion do that asphaltenes suffer some limitations and cannot leave the pore easily experiencing over cracking which can lead to higher coke formation in the pores.

Table 3
Spent catalysts composition and reduction in textural properties due to the deposited species

Catalyst	Deposited species (wt.%)			Percentage of reduction in textural properties	
	V	Ni	C	SSA	PV
CoMo/Mg–Al-0.01	1.5	0.4	10.12	64	56
CoMo/Mg–Al-0.1	3.1	0.6	8.23	47	52

6. Conclusion

Large pore magnesia–alumina mixed oxide supports with even distribution of MgO were prepared using homogeneous precipitation method. The MgO nano-crystals were uniformly distributed in the Al_2O_3 matrix. MgO–Al_2O_3 supported CoMo catalysts prepared with chelating agents showed enhanced activity for thiophene HDS using calcinations before sulfidation. The calcination effect may contribute to the nature of MgO interaction with the chelating agent during the preparation of the catalyst that facilitates an easy sulfidation due to a weak interaction of Mo with the support, which turn them into more active catalysts. The results of Raman spectroscopy confirm that the chelating agent avoid formation of Co_3O_4 and $CoMoO_4$ rather it promotes to Mo interaction over the magnesia–alumina support loading to the formation of $MgMoO_4$ species, those are the easy species to convert into MoS_2 during the sulfidation.

Different MgO content supported catalysts were evaluated for hydrotreating of Maya heavy crude oil and the effects of support composition were observed for HDS, HDM and HDAs reactions, that are referred to high hydrogenolysis and lower hydrogenation functions. The higher the MgO content the better the stability of the catalyst that also corresponds to the larger pore diameter of the catalyst.

Acknowledgments

We thank to Dr. Carlos Angeles for HRTEM analysis. One of us F. Trejo thanks to CONACyT for a post-doctorate fellowship.

References

[1] G. Muralidhar, F.E. Massoth, J. Shabtai, J. Catal. 85 (1984) 44.
[2] F.E. Massoth, G. Muralidhar, J. Shabtai, J. Catal. 85 (1984) 53.
[3] E.J.M. Hensen, V.H.J. de Beer, J.A.R. van Veen, R.A. van Santen, Catal. Lett. 84 (2002) 59.
[4] M.S. Rana, M.L. Huidobro, J. Ancheyta, M.T. Gómez, Catal. Today 107/108 (2005) 346.
[5] J. Ancheyta, M.S. Rana, E. Furimsky, Catal. Today 109 (2005) 3.
[6] M. Breysse, P. Afanasiev, C. Geantet, M. Vrinat, Catal. Today 86 (2003) 5.
[7] B. Caloch, M.S. Rana, J. Ancheyta, Catal. Today 98 (2004) 91.
[8] F. Aberuagba, M. Kumar, J.K. Gupta, G. Muralidhar, L.D. Sharma, React. Kinet. Catal. Lett. 75 (2002) 245.
[9] T. Klicpera, M. Zdražil, J. Catal. 206 (2002) 314.
[10] T. Klimova, D. Solís, J. Ramírez, Catal. Today 43 (1998) 135.
[11] R. Cattaneo, T. Shido, R. Prins, J. Catal. 185 (1999) 199.
[12] R. Cattaneo, T. Weber, T. Shido, R. Prins, J. Catal. 191 (2000) 225.
[13] R. Cattaneo, F. Rota, R. Prins, J. Catal. 199 (2001) 318.
[14] K. Al-Dalama, A.A. Stanislaus, Energy Fuels 20 (2006) 1777.
[15] T. Shimizu, K. Hiroshima, T. Honma, T. Mochizuki, M. Yamada, Catal. Today 45 (1998) 271.
[16] Y. Yoshimura, T. Sato, H. Shimada, N. Matsubayashi, M. Imamura, A. Nishijima, M. Higo, S. Yoshitomi, Catal. Today 29 (1996) 221.
[17] A.I. Tsyganok, M. Inaba, T. Tsunoda, S. Hamakawa, K. Suzuki, T. Hayakawa, Catal. Commun. 4 (2003) 493.
[18] P. Blanchard, C. Mauchausse, E. Payen, J. Grimblot, O. Poulet, N. Boisdron, R. Loutaty, Stud. Surf. Sci. Catal. 91 (1995) 1037.
[19] A.J. van Dillen, R.J.A.M. Terörde, D.J. Lensveld, J.W. Geus, K.P. de Jong, J. Catal. 216 (2003) 257.
[20] J.A.R. van Veen, E. Gerkema, A.M. van der Kraan, P.A.J.M. Hendriks, H. Beens, J. Catal. 133 (1992) 112.
[21] J.A.R. van Veen, E. Gerkema, A.M. van der Kraan, A. Knoester, J. Chem. Soc., Chem. Commun. 22 (1987) 1684.
[22] G. Kishan, L. Coulier, V.H.J. de Beer, J.A.R. van Veen, J.W. Niemantsverdriet, J. Catal. 196 (2000) 180.
[23] G. Kishan, L. Coulier, J.A.R. van Veen, J.W. Niemantsverdriet, J. Catal. 200 (2001) 194.
[24] G. Kishan, J.A.R. van Veen, J.W. Niemantsverdriet, Top. Catal. 29 (2004) 103.
[25] L. Coulier, V.H.J. de Beer, J.A.R. van Veen, J.W. Niemantsverdriet, J. Catal. 197 (2001) 26.
[26] H. Itou, N. Koizumi, N. Sakamoto, T. Honma, M. Shingu, M. Yamada, J. Jpn. Pet. Inst. 47 (2004) 249.
[27] H. Itou, N. Koizumi, N. Sakamoto, T. Honma, K. Ogawa, M. Shingu, M. Yamada, J. Jpn. Pet. Inst. 47 (2004) 258.
[28] N. Koizumi, Y. Murata, N. Sakamoto, H. Itou, M. Yamada, J. Jpn. Pet. Inst. 48 (2005) 344.
[29] N. Koizumi, M. Shingu, K. Hata, Y. Murata, H. Itou, M. Yamada, M. Prepr. Am. Chem. Soc., Div. Pet. Chem. 49 (2004) 292.
[30] Y. Okamoto, S.Y. Ishihara, M. Kawano, M. Satoh, T. Kubota, J. Catal. 217 (2003) 12.
[31] M. Sun, D. Nicosia, R. Prins, Catal. Today 86 (2003) 173.
[32] M. Yamada, Prep. Am. Chem. Soc., Div. Pet. Chem. 49 (2004) 287.
[33] V. Sundaramurthy, A.K. Dalai, J. Adjaye. Catal. Lett. 102 (2005) 299.
[34] L.G. Silen, A.E. Martell, Stability constants of metal complexes, Chem. Soc., Lond. 17 (1964) 4.
[35] H. Shimada, T. Sato, Y. Yoshimura, J. Hiraishi, A. Nishijima, J. Catal. 110 (1988) 275.
[36] J.M. Stencel, L.E. Makovsky, T.A. Sarkus, J. de Vries, R. Thomas, J.A. Moulijn, J. Catal. 90 (1984) 314.
[37] M.C. Abello, M.F. Gomez, L.E. Cadús, Ind. Eng. Chem. Res. 35 (1996) 2137.
[38] W.P. Griffith, Coord. Chem. Rev. 5 (1970) 459.
[39] S.C. Chang, M.A. Leugers, S.R. Bare, J. Phys. Chem. 96 (1992) 10358.
[40] M.S. Rana, J. Ramírez, A. Gutiérrez-Alejandre, J. Ancheyta, L. Cedeño, S.K. Maity, J. Catal. 246 (2007) 100.
[41] R. Cattaneo, T. Shido, R. Prins, Stud. Surf. Sci. Catal. 127 (1999) 421.
[42] J. Ramírez, M.S. Rana, J. Ancheyta, Characteristics of heavy oil hydroprocessing catalysts, in: J. Ancheyta, J.G. Speight (Eds.), Hydroprocessing of Heavy Oils and Residua, Taylor & Francis, Boca Raton, 2007 (Chapter 6).
[43] M.S. Rana, J. Ancheyta, P. Rayo, S.K. Maity, Catal. Today 98 (2004) 151.
[44] M. Absi-Halabi, A. Stanislaus, T. Al-Mughni, S. Khan, A. Qamra, Fuel 74 (1995) 1211.
[45] B.J. Smith, J. Wei, J. Catal. 132 (1991) 21.
[46] J. Cinibulk, P.J. Kooyman, Z. Vit, M. Zdražil, Catal. Lett. 89 (2003) 147.